JOC The Journal of Organic Chemistry

Article

pubs.acs.org/joc

Effect of Extended π Conjugation on the Spectroscopic and Electrochemical Properties of Boron Difluoride Formazanate Complexes

Stephanie M. Barbon, Viktor N. Staroverov, and Joe B. Gilroy*

Department of Chemistry and the Centre for Advanced Materials and Biomaterials Research (CAMBR), The University of Western Ontario, 1151 Richmond Street North, London, Ontario, Canada N6A 5B7

Supporting Information

ABSTRACT: The effect of extended π conjugation on the spectroscopic and electrochemical properties of boron difluoride (BF_2) formazanate complexes was studied by the systematic comparison of phenyl- and naphthyl-substituted derivatives. Each of the BF_2 complexes described was characterized by ^{1}H, ^{13}C, ^{11}B, and ^{19}F NMR spectroscopy, cyclic voltammetry, infrared spectroscopy, UV−vis absorption and emission spectroscopy, and mass spectrometry. X-ray crystallography and electronic structure calculations were used to rationalize the trends observed, including direct comparison of 3-cyano-, 3-nitro-, and 3-phenyl-substituted BF_2 formazanate complexes. In all cases, the wavelengths of maximum absorption and emission were red-shifted as π conjugation was systematically extended (by replacing phenyl with naphthyl), fluorescence quantum yields increased (up to 10-fold), and electrochemical conversion of the formazanate complexes to their radical anion and dianion forms occurred at less negative potentials (easier to reduce).

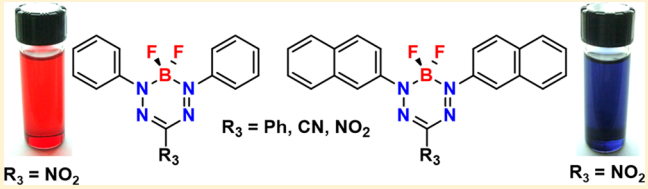

INTRODUCTION

It has long been known that extended π conjugation has a drastic effect on the electronic properties and spectroscopic features of molecules containing fused aromatic rings. Perhaps the simplest molecules that demonstrate this behavior are benzene, naphthalene, and anthracene. In this series, as the extent of π conjugation increases, the wavelength of maximum absorption also increases, from ∼260 nm for benzene to ∼310 nm for naphthalene and ∼375 nm for anthracene.[1] The emission quantum yields of these compounds follow the same trend, increasing from 0.053 in benzene to 0.19 and 0.27 in naphthalene and anthracene, respectively.[1] As the structures of π-conjugated molecules become increasingly complex, so do their electronic properties, which often leads to their use in a variety of applications. pi-Conjugated molecules are frequently employed in photovoltaic cells,[2] as luminescent materials,[3] in field-effect transistors,[4] and as materials exhibiting aggregation-induced emission.[5]

Among the most widely studied π-conjugated molecular materials are boron difluoride (BF_2) complexes of N,N-, O,O-, and N,O-chelating ligands.[3,6] Boron dipyrromethenes (BODIPYs) are by far the most common of this class of complexes.[7,8] BODIPY **1**, which was first reported by Daub and co-workers in 1998, showed absorption and emission maxima around 500 nm, with an emission quantum yield of 0.60.[9] Ono et al. synthesized compound **2**, which is structurally very similar to **1** but includes a greater degree of π conjugation. The addition of two fused phenyl rings increased the wavelength of maximum absorption and emission by close to 100 nm and the quantum yield to 0.91.[10] Similarly, Fu's group has applied this strategy to their naphthyridine BF_2 complexes **3** and **4** and observed that by extending the conjugation of the naphthyridine ligand by a pyridine moiety, the solid-state fluorescence quantum yield increased by 0.20, and the wavelength of maximum absorption and emission was red-shifted by more than 20 nm.[11] Piers et al. have modified the structure of anilido-pyridine ligands to study the properties of the BF_2 complexes of both the parent anilido-pyridine complex **5** and the modified BF_2 complex **6**, which has a higher degree of π conjugation. This modification nearly doubled the emission quantum yield from 0.33 to 0.60 and red-shifted the absorption and emission maxima by ca. 50 nm.[12]

The Gilroy and Otten groups have recently shown that BF_2 complexes **7** derived from formazans[13] **8** have desirable spectroscopic and electrochemical properties that are easily tuned through structural variation.[14] In general, electron-withdrawing substituents were shown to increase reduction potentials (E°_{red1} and E°_{red2} become less negative) associated with radical anion and dianion formation and blue-shift the wavelength of maximum absorption and emission in comparison to phenyl-substituted analogues. Electron-donating substituents had the opposite effect, decreasing the reduction potentials (E°_{red1} and E°_{red2} become more negative), red-shifting the wavelength of maximum absorption and emission, and increasing emission intensities. We have also recently demonstrated efficient electrochemiluminescence from a *p*-anisole-substituted boron difluoride formazanate complex (**7**: $Ar_1 = Ar_5 = p\text{-}C_6H_4OMe$, $R_3 = CN$).[15]

Received: March 18, 2015
Published: May 6, 2015

DOI: 10.1021/acs.joc.5b00620
J. Org. Chem. 2015, 80, 5226−5235

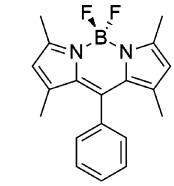

1
λ_{max} = 497 nm
λ_{em} = 505 nm
ϕ = 0.60

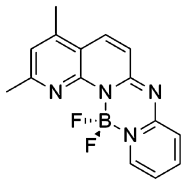

3
λ_{max} = 422 nm
λ_{em} = 527 nm
ϕ = 0.44

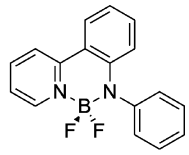

5
λ_{max} = 417 nm
λ_{em} = 531 nm
ϕ = 0.33

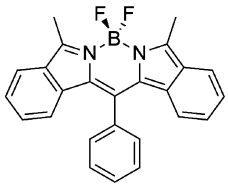

2
λ_{max} = 597 nm
λ_{em} = 606 nm
ϕ = 0.91

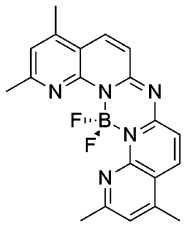

4
λ_{max} = 445 nm
λ_{em} = 557 nm
ϕ = 0.64

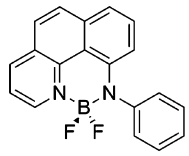

6
λ_{max} = 465 nm
λ_{em} = 584 nm
ϕ = 0.60

In an effort to assess the effect of extended π conjugation on the properties of BF_2 formazanate dyes, and taking advantage of the ease of structural variation of the formazanate backbone, we have synthesized the series of formazans **8a–h** and BF_2 complexes **7a–h** by systematically introducing naphthyl (Np) substituents at the 1-, 3-, and 5-positions of the formazanate backbone.

RESULTS AND DISCUSSION

Synthesis. Triarylformazans **8a–d**, 3-cyanoformazans **8e,f**, and 3-nitroformazans **8g,h** were synthesized by adapting previously published protocols.[16] Formazanate BF_2 complexes **7a–h** were prepared by refluxing the parent formazans in toluene in the presence of excess triethylamine and boron trifluoride diethyl etherate (Scheme 1 and Table 1).[14b,c] Analysis by ^{1}H, ^{11}B, ^{13}C, and ^{19}F NMR spectroscopy (Figures S1–S24 in the Supporting Information), mass spectrometry, and IR spectroscopy confirmed the proposed structures of formazans **8a–h** and BF_2 complexes **7a–h**. The bidentate coordination mode observed for the formazanate ligands was consistent with other complexes of boron[14,17] and transition metals.[18]

Naphthyl-Substituted BF_2 Formazanate Complexes. By comparison of 1,3,5-triphenyl-substituted BF_2 complex **7a** with naphthyl-substituted complexes **7b–d**, the effect of π conjugation on the properties of BF_2 triarylformazanate complexes was explored. Molar absorptivities associated with $\pi \rightarrow \pi^*$ transitions in **7a–d** ranged from 20900 to 26800 M^{-1} cm^{-1} in toluene. The replacement of one phenyl substituent for a naphthyl substituent in **7b** (Ar_1 = Ar_5 = Ph, R_3 = Np) and **7c** (Ar_1 = R_3 = Ph, Ar_5 = Np) caused a red shift of maximum absorption (λ_{max}) in toluene, from 517 nm for **7a** to 529 nm for **7b** and 535 nm for **7c**. The replacement of a second phenyl substituent in **7d** (Ar_1 = Ar_5 = Np, R_3 = Ph) resulted in a further red shift in λ_{max} to 556 nm (Figure 1a, Figures S25 and S26 in the Supporting Information, and Table 2). In order to verify that the observed absorption properties were not simply due to the presence of a naphthyl group, the UV–vis absorption spectrum of 2-naphthylamine was recorded (λ_{max} 345 nm, Figure S27 in the Supporting Information). Interestingly, on comparison of compounds **7b,c**, which each have one naphthyl and two phenyl substituents, **7c** has a slightly longer wavelength of maximum absorption (529 vs 535 nm).

All four compounds are weakly emissive, with maximum emission (λ_{em}) observed between 626 and 681 nm (Figure 1b, Figures S25 and S26 in the Supporting Information, and Table 2). The trend observed for the wavelengths of maximum absorption is mirrored here, with the λ_{em} values of **7b–d** being red-shifted with respect to **7a**. Quantum yields for all four complexes are below 0.05. However, the observed Stokes shifts (ν_{ST}) were large (**7a**, ν_{ST} 109 nm, 3368 cm^{-1}; **7b**, ν_{ST} 124 nm, 3590 cm^{-1}; **7c**, ν_{ST} 124 nm, 3517 cm^{-1}; **7d**, ν_{ST} 125 nm, 3301 cm^{-1}).

Complexes **7a–d** (six π electrons) are electrochemically active, exhibiting two reversible one-electron reduction waves corresponding to the reversible formation of ligand-centered radical anions (seven π electrons) and dianions (eight π electrons), respectively (Figure 2, Table 2). Closely related Kuhn-type verdazyls **9** and 6-oxoverdazyls **10** (seven π electrons), which also benefit from significant delocalization and stabilized frontier molecular orbitals due to the presence of four nitrogen atoms in their heterocyclic backbones, exhibit similar redox behavior and can be reversibly oxidized to cations (six π electrons) and anions (eight π electrons).[16c] The reduction potentials observed for **7a–d** become less negative (easier to reduce) as naphthyl substituents are introduced (**7a**, −0.82 and −1.89 V; **7b**, −0.81 and −1.88 V; **7c**, −0.80 and −1.85 V; **7d**, −0.78 and −1.78 V). This trend is consistent with naphthyl substituents having stabilized LUMOs due to

Table 1. Substituents for Formazans 8a–i and BF_2 Formazanate Complexes 7a–i

	Ar_1	Ar_5	R_3
a	Ph	Ph	Ph
b	Ph	Ph	Np
c	Ph	Np	Ph
d	Np	Np	Ph
e[14b]	Ph	Ph	CN
f	Np	Np	CN
g	Ph	Ph	NO_2
h	Np	Np	NO_2
i[14a]	Ph	Ph	*p*-tolyl

Scheme 1. Synthesis of BF_2 Formazanate Complexes

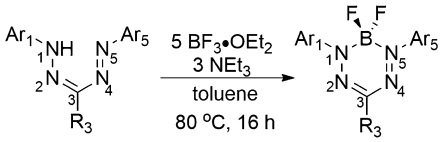

8 **7**

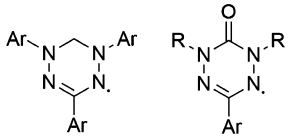

9 **10**

Ar = Ph, *p*-substituted Ph
R = Me, *i*Pr

DOI: 10.1021/acs.joc.5b00620
J. Org. Chem. 2015, 80, 5226–5235

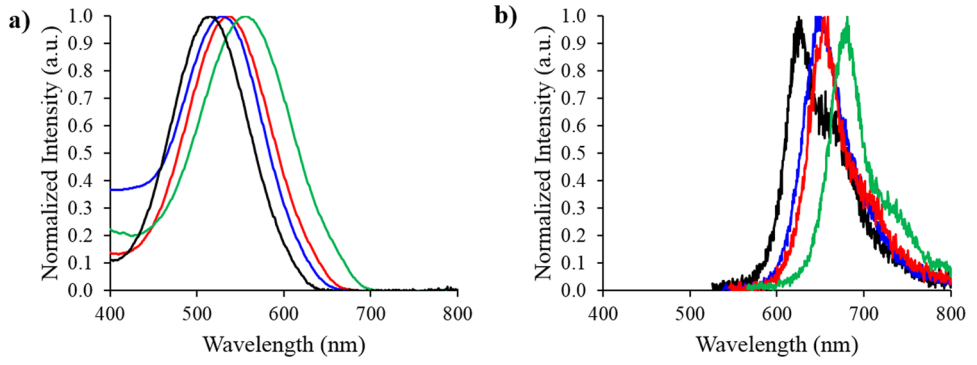

Figure 1. UV−vis absorption spectra (a) and emission spectra (b) of **7a** (black, $Ar_1 = Ar_5 = R_3 = Ph$), **7b** (blue, $Ar_1 = Ar_5 = Ph$, $R_3 = Np$), **7c** (red, $Ar_1 = R_3 = Ph$, $Ar_5 = Np$), and **7d** (green, $Ar_1 = Ar_5 = Np$, $R_3 = Ph$) recorded for 10^{-5} M degassed toluene solutions.

Table 2. Solution Characterization Data for BF_2 Complexes 7a−h

	solvent	λ_{max} (nm)	ε (M^{-1} cm^{-1})	λ_{em} (nm)	Φ_f[a]	ν_{ST} (nm)	ν_{ST} (cm^{-1})	E°_{red1}[b] (V)	E°_{red2}[b] (V)
7a	THF	509	22500	627	0.01	118	3697	−0.82	−1.89
	toluene	517	23800	626	<0.01	109	3368		
	CH_2Cl_2	509	23400	630	0.01	121	3773		
7b	THF	522	22000	658	0.01	136	3960	−0.81	−1.88
	toluene	529	20900	653	<0.01	124	3590		
	CH_2Cl_2	524	20300	656	0.09	132	3840		
7c	THF	529	25000	655	<0.01	126	3636	−0.80	−1.85
	toluene	535	26800	659	0.02	124	3517		
	CH_2Cl_2	530	27500	656	0.03	126	3624		
7d	THF	550	22900	680	0.02	130	3476	−0.78	−1.78
	toluene	556	25200	681	0.05	125	3301		
	CH_2Cl_2	551	23600	682	<0.01	131	3486		
7e[14b]	THF	489	25400	585	0.05	96	3356	−0.53	−1.68
	toluene	502	30400	586	0.15	84	2855		
	CH_2Cl_2	491	34600	584	0.09	93	3243		
7f	THF	551	27700	676	0.25	125	3356	−0.49	−1.54
	toluene	581	25700	670	0.39	89	2286		
	CH_2Cl_2	558	23900	669	0.32	111	2973		
7g	THF	487	21000	585	0.03	98	3440	−0.48	−1.61
	toluene	505	26000	590	0.05	85	2853		
	CH_2Cl_2	488	29200	587	0.03	99	3456		
7h	THF	561	27500	679	0.23	118	3098	−0.45	−1.49
	toluene	583	24100	671	0.48	88	2250		
	CH_2Cl_2	563	26700	677	0.28	114	2991		

[a]Quantum yields were measured according to a previously reported method[19] using ruthenium tris(bipyridine) hexafluorophosphate as a relative standard[20] and corrected for detector nonlinearity (Figure S29 in the Supporting Information). [b]Cyclic voltammetry experiments were conducted in acetonitrile containing 1 mM analyte and 0.1 M tetrabutylammonium hexafluorophosphate at a scan rate of 100 mV s^{-1}. All voltammograms were referenced internally against the ferrocene/ferrocenium redox couple.

enhanced π conjugation in comparison to phenyl substituents. A single naphthyl substituent at the 1,5-position has a more drastic effect than the same substituent at the 3-position, as **7c** is easier to reduce than **7b** by approximately 13 mV. Each complex also undergoes irreversible oxidation within the electrochemical window (Figure S28 in the Supporting Information).

The data collected for compounds **7a−d** allow for the conclusion that extended π conjugation has a dramatic effect on the properties of BF_2 formazanate complexes. Systematically extending π conjugation increases the emission quantum yields, red-shifts the wavelengths of maximum absorption and emission, and raises the reduction potentials of the resulting compounds. It is noteworthy that these data also demonstrate that extending the π conjugation at the 3-position of the formazanate backbone has a less pronounced effect than similar structural modification at the 1,5-positions (see below).

3-Phenyl-, 3-Cyano-, and 3-Nitro-Substituted BF_2 Formazanate Complexes. The influence of cyano-, nitro-, and phenyl-substituents at the R_3 position of the formazanate backbone on the properties of BF_2 formazanate dyes was assessed through comparison of 1,5-diphenyl-substituted compounds **7a** (R_3 = Ph), **7e** (R_3 = CN), and **7g** (R_3 = NO_2). Single crystals of complex **7g** were grown by slow evaporation of a concentrated dichloromethane solution (Figure 3). The solid-state structure of complex **7e** has previously been reported.[14b] Attempts to crystallize complex **7a** under a variety of conditions consistently resulted in weakly diffracting, multiply twinned crystals (likely due to the pseudo-3-fold symmetry of **7a**) unsuitable for X-ray diffraction studies. Therefore, complex **7i** ($Ar_1 = Ar_5 = Ph$, R_3 = *p*-tolyl), previously

DOI: 10.1021/acs.joc.5b00620
J. Org. Chem. 2015, 80, 5226−5235

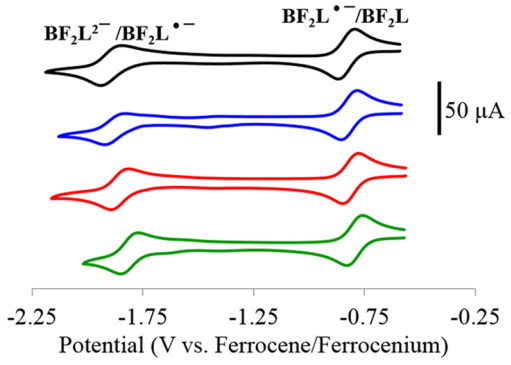

Figure 2. Cyclic voltammograms of **7a** (black, $Ar_1 = Ar_5 = R_3 = Ph$), **7b** (blue, $Ar_1 = Ar_5 = Ph$, $R_3 = Np$), **7c** (red, $Ar_1 = R_3 = Ph$, $Ar_5 = Np$), and **7d** (green, $Ar_1 = Ar_5 = Np$, $R_3 = Ph$), recorded at 100 mV s^{-1} in 1 mM acetonitrile solutions containing 0.1 M tetrabutylammonium hexafluorophosphate as supporting electrolyte. L = redox-active formazanate ligand.

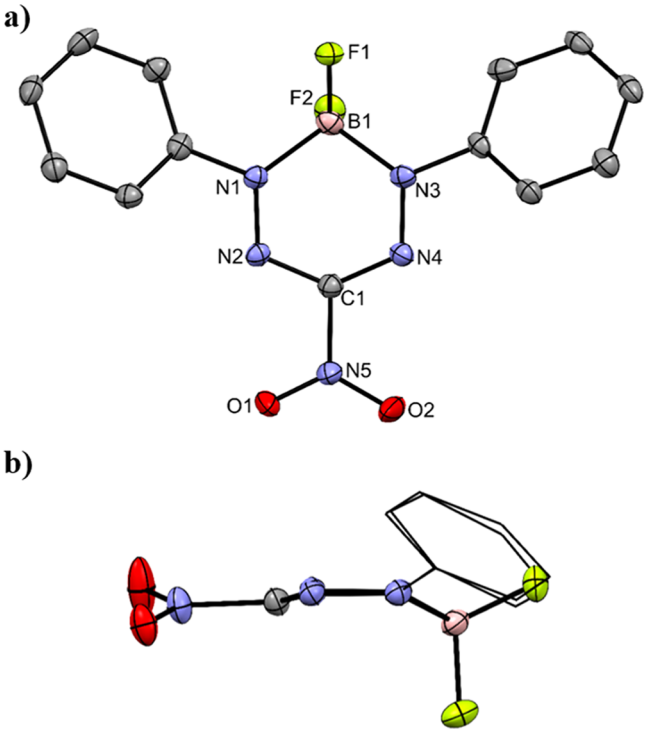

Figure 3. (a) Top view and (b) side view of the solid-state structure of BF_2 formazanate complex **7g**. Thermal ellipsoids are shown at the 50% probability level and hydrogen atoms have been removed for clarity. Only one of two structurally similar molecules in the asymmetric unit for **7g** is shown.

reported by the Otten group,[14a] has been included for comparison, as the structural metrics associated with the presence of a single *p*-tolyl substituent are not expected to differ significantly from those for complex **7a**. All three BF_2 complexes contain a four-coordinate boron center in a distorted-tetrahedral geometry, which is slightly displaced from the plane of the formazanate backbone (−N═N−C═N−N−). It is also noteworthy that the formazanate backbone is delocalized in all three examples (Table 3) with the CN and NN bond lengths falling between typical single and double bonds for the respective atoms involved.[21] Each complex possesses moderate degrees of twisting between the *N*-aryl substituents and the formazanate backbone (**7e**, 22.0° and 24.4°; **7g**, 36.4° and 38.2°; **7i**, 48.0° and 42.0°). Overall we can conclude that, structurally, all three complexes are very similar, and the nature of the R_3 substituent has little influence over the bond lengths and angles of the BF_2 formazanate heterocycle (Table 3).

Table 3. Selected Bond Lengths (Å) and Angles (deg) for BF_2 Formazanate Complexes 7e,g and 7i[14a] Determined by Single-Crystal X-ray Diffraction

	7e[14b]	7g[a]	7i[b,14a]
N1−N2, N3−N4	1.2900(15), 1.2948(15)	1.302(5), 1.304(5)	1.308(1), 1.308(1)
C1−N2, C1−N4	1.3408(17), 1.3379(17)	1.330(5), 1.318(5)	1.346(1), 1.343(1)
N1−B1, N3−B1	1.5748(18), 1.5771(17)	1.576(6), 1.563(6)	1.559(2), 1.552(2)
N1−B1−N3	105.55(10)	103.4(3)	102.40(9)
N2−N1−B1, N4−N3−B1	124.78(10), 124.32(11)	121.5(3), 122.2(3)	121.45(9), 121.69(9)
N2−C1−N4	129.33(12)	130.0(4)	124.2(1)
C1−N2−N1, C1−N4−N3	117.14(11), 117.30(11)	115.6(3), 115.5(3)	117.68(9), 117.72(9)
boron displacement[c]	0.192	0.456	0.500
dihedral angle[d]	18.7, 26.2	36.4, 38.2	48.0, 42.0

[a]The second molecule in the unit cell of **7g** has very similar structural metrics. [b]The numbering convention for the structure previously reported by Otten and co-workers[14a] has been modified for ease of comparison. [c]Distance between B1 and N_4 plane. [d]Angles between the plane defined by the N1 and N3 aryl substituents and the N_4 plane.

As both cyano and nitro groups are strongly electron-withdrawing, complexes **7e,g** have similar spectroscopic and electrochemical properties, though they differ significantly in comparison to complex **7a**. All three complexes are strongly absorbing between 400 and 600 nm ($\pi \rightarrow \pi^*$), though their λ_{max} values range from 502 nm (**7e**) to 505 nm (**7g**) and 517 nm (**7a**) (Figure 4a, Figures S30 and S31 in the Supporting Information, and Table 2). While all three phenyl-substituted complexes are fluorescent (Figure 4b and Table 2), their emission quantum yields in toluene vary dramatically (**7a**, λ_{em} 626 nm, Φ = <0.01; **7e**, λ_{em} 586 nm, Φ = 0.15; **7g**, λ_{em} 590 nm, Φ = 0.05). We assume that the difference in quantum yields is likely due to nonradiative decay pathways associated with the 3-phenyl substituent. While complex **7a** has the lowest quantum yield, it has the largest Stokes shift (ν_{ST} 109 nm, 3368 cm^{-1}) in toluene, significantly higher than those of complexes **7e** (ν_{ST} 84 nm, 2855 cm^{-1}) and **7g** (ν_{ST} 85 nm, 2853 cm^{-1}). Given the qualitative similarities of the emission spectra in different solvents (Figures S25, S26, S30, and S31 in the Supporting Information), we believe that the low-energy shoulders observed can be attributed to vibrational overtones rather than aggregation.

Finally, the electron-withdrawing nature of the R_3 substituent has a significant effect on the electrochemical properties of BF_2 formazanate complexes. Complex **7g** ($R_3 = NO_2$) is the easiest to reduce, with the first and second one-electron reductions occurring at −0.48 and −1.61 V vs ferrocene/ferrocenium. Complex **7e** (R_3 = CN) is slightly more difficult to reduce at potentials of −0.53 and −1.68 V. Finally, complex **7a** (R_3 = Ph) is substantially more difficult to reduce, with the sequential one-electron reductions occurring at −0.82 and −1.89 V (Figure S32 in the Supporting Information and Table 2).

As mentioned earlier, the properties of complexes bearing phenyl and naphthyl substituents at the 3-position of the

DOI: 10.1021/acs.joc.5b00620
J. Org. Chem. 2015, 80, 5226−5235

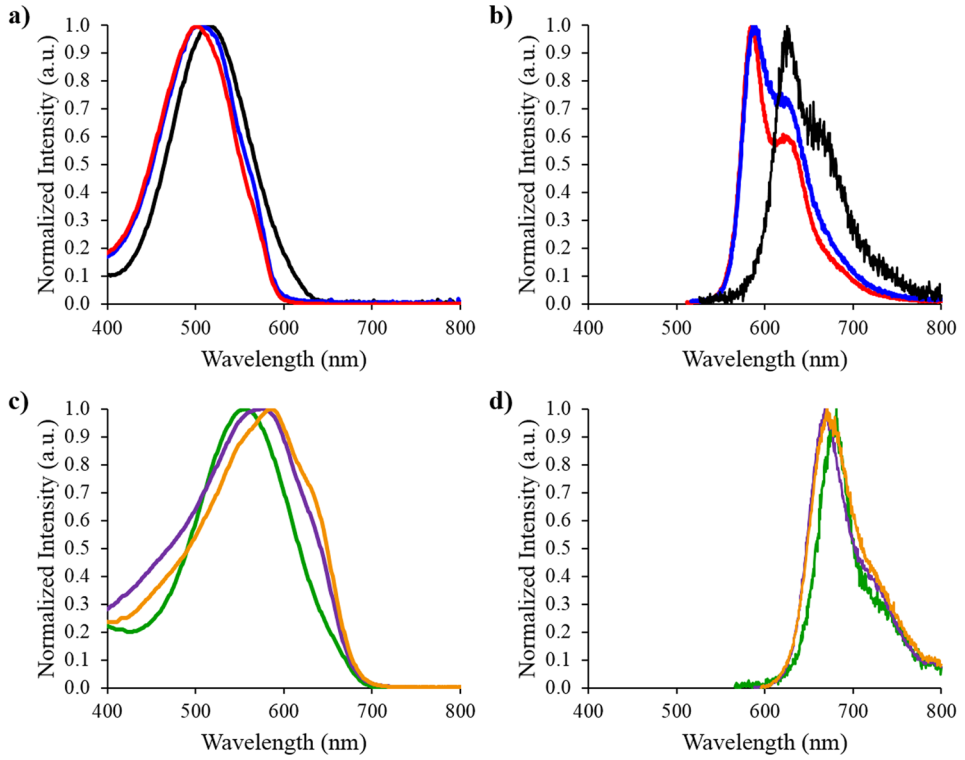

Figure 4. UV−vis absorption spectra (a) and emission spectra (b) of **7a** (black, $Ar_1 = Ar_5 = R_3 = Ph$), **7e** (red, $Ar_1 = Ar_5 = Ph$, $R_3 = CN$), and **7g** (blue, $Ar_1 = Ar_5 = Ph$, $R_3 = NO_2$). UV−vis absorption spectra (c) and emission spectra (d) of **7d** (green, $Ar_1 = Ar_5 = Np$, $R_3 = Ph$), **7f** (purple, $Ar_1 = Ar_5 = Np$, $R_3 = CN$), and **7h** (orange, $Ar_1 = Ar_5 = Np$, $R_3 = NO_2$) recorded for 10^{-5} M degassed toluene solutions.

formazanate backbone did not differ dramatically. We have also previously shown that the substitution of electron-donating and -withdrawing groups introduced on aryl rings at the 3-position of the formazanate backbone did not significantly alter the properties of the resulting BF_2 complexes.[14c] However, complexes **7a,e,g** clearly demonstrate that the same trend is not true for all substituents at the 3-position, as the properties of **7e** ($R_3 = CN$) and **7g** ($R_3 = NO_2$) are drastically different from those of **7a** ($R_3 = Ph$). This is likely due to the strong electron-withdrawing characteristics of the cyano and nitro substituents and related less to the extent of π conjugation in these complexes.

By comparison of naphthyl-substituted complexes **7d,f,h** with phenyl-substituted complexes **7a,e,g**, the effect of π conjugation on the properties of BF_2 3-phenyl-, 3-cyano-, and 3-nitro-formazanate complexes was studied. The wavelength of maximum absorption of naphthyl-substituted complexes **7d,f,h** were red-shifted (relative to the phenyl-substituted analogues **7a,e,g**), from 502 to 581 nm for complex **7f** ($R_3 = CN$), from 505 to 583 nm for complex **7h** ($R_3 = NO_2$), and from 517 to 556 nm for complex **7d** ($R_3 = Ph$) (Figure 4c and Table 2). While in all three cases the observed trend was the same, the magnitude of the red shift upon replacement of two phenyl substituents with two naphthyl substituents was much greater for complexes with strongly electron-withdrawing R_3 substituents ($\Delta\lambda_{max}$ 79 nm, 2709 cm^{-1} ($R_3 = CN$); $\Delta\lambda_{max}$ 78 nm, 2649 cm^{-1} ($R_3 = NO_2$); $\Delta\lambda_{max}$ 39 nm, 1357 cm^{-1} ($R_3 = Ph$)).

The emission spectra of complexes **7d,f,h** (Figure 4d and Table 2) were also red-shifted with respect to the phenyl-substituted analogues, with λ_{em} values of 681 nm (**7d**), 670 nm (**7f**), and 671 nm (**7g**) in toluene. The emission quantum yields of these three complexes were significantly higher than the quantum yields of the phenyl-substituted complexes. The addition of the naphthyl substituent increases the emission quantum yield for **7d** to 0.05 (from <0.01 in complex **7a**), for **7f** to 0.39 (from 0.15 in complex **7e**), and for **7h** to 0.48 (from 0.05 in complex **7g**). The Stokes shifts observed for the 3-cyano- and 3-nitro-substituted complexes were smaller than those of 3-phenyl-substituted complexes. All complexes with R_3 = CN and NO_2 have Stokes shifts ranging from 84 to 89 nm (2250−2855 cm^{-1}) in toluene, while those with $R_3 = Ph$ have generally larger Stokes shifts, from 109 to 125 nm (3368−3590 cm^{-1}) in toluene.

The cyclic voltammograms of complexes **7d,f,h** demonstrate that the more electron-deficient complexes **7f,h** are significantly easier to reduce (by almost 0.300 V) than complex **7d** (Figure 5 and Table 2). In all three examples, the reduction potential of the naphthyl-substituted complexes was 0.030−0.045 V higher than that of the phenyl-substituted analogues. Complexes **7f−h** also underwent irreversible oxidation within the electrochemical window of the solvent (CH_3CN) (Figure S33 in the Supporting Information).

Electronic Structure Calculations. In an attempt to rationalize the trends observed, we calculated the highest occupied and lowest unoccupied molecular orbitals (HOMOs and LUMOs) of **7a,e,g** (Figure 6 and Table 4) with the Gaussian 09 program[22] using the M06 density functional[23] and the 6-311+G* basis set, in vacuum and in toluene solution. The Kohn−Sham molecular orbitals of **7a,e,g** were computed for the corresponding optimized molecular structures. The Ultra-Fine integration grid was employed in all calculations. Solvation effects were treated implicitly using the polarizable continuum model (SCRF=PCM). All optimized structures of **7a,e,g** have C_s symmetry and were confirmed by vibrational analysis to be minima on the potential energy surface, both in vacuum and in

DOI: 10.1021/acs.joc.5b00620
J. Org. Chem. 2015, 80, 5226−5235

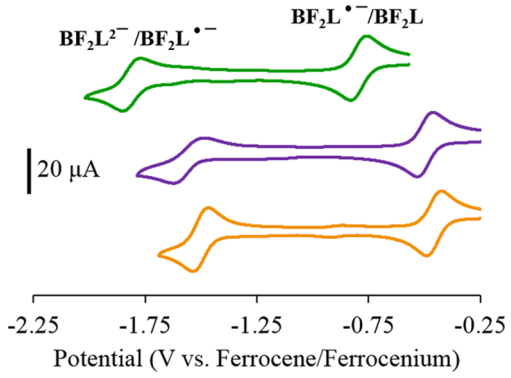

Figure 5. Cyclic voltammograms of **7d** (green, $Ar_1 = Ar_5$ = Np, R_3 = Ph), **7f** (purple, $Ar_1 = Ar_5$ = Np, R_3 = CN), and **7h** (orange, $Ar_1 = Ar_5$ = Np, $R_3 = NO_2$). Cyclic voltammograms were recorded at 100 mV s^{-1} in 1 mM acetonitrile solutions containing 0.1 M tetrabutylammonium hexafluorophosphate as supporting electrolyte.

toluene solution (see the Supporting Information for further details). Time-dependent density-functional theory (DFT) studies have confirmed the HOMO and LUMO to be the dominant orbital pair involved in the lowest energy transition in complexes **7a,e,g** (see Table 4).

The calculated LUMOs for complexes **7a,e,g** are highly delocalized over the formazanate backbone and *N*-aryl substituents but do not extend over the 3-substituents. In contrast, the HOMOs are delocalized over both the *N*-aryl and 3-substituents (Ph, CN, and NO_2). The electrochemical reduction of complexes **7a,e,g** should primarily involve the LUMOs of each complex. Solely on the basis of the shape of the calculated frontier orbitals, the reduction potentials for each compound should be similar. However, due to the differing electron-withdrawing characteristics of the 3-subsituents, the HOMO/LUMO energies and the experimentally determined reduction potentials varied significantly. The observed trend in the first and second reduction potentials (E°_{red1} and E°_{red2}), which involves stepwise population of the LUMO, was consistent with the trend in computed LUMO energies (ε_{LUMO}) in toluene solution: **7g** (−3.83 eV) < **7e** (−3.76 eV) < **7a** (−3.30 eV).

Table 4. Electronic Excitation and HOMO/LUMO Energies of BF_2 Complexes 7a ($Ar_1 = Ar_5 = R_3$ = Ph), 7e ($Ar_1 = Ar_5$ = Ph, R_3 = CN) and 7g ($Ar_1 = Ar_5$ = Ph, $R_3 = NO_2$) under Vacuum and in Toluene Solution Calculated at the M06/6-311+G* Level of Theory using the SCRF Method

	lowest excitation energy[a]		orbital energy		HOMO−LUMO gap	
compound	ΔE (eV)	ΔE (nm)	ε_{HOMO} (eV)	ε_{LUMO} (eV)	$\Delta\varepsilon$ (eV)	$\Delta\varepsilon$ (nm)
			Vacuum			
7a	2.56	484	−6.38	−3.25	3.13	397
7e[14b]	2.76	448	−7.12	−3.79	3.34	372
7g	2.79	444	−7.24	−3.85	3.39	366
			Toluene Solution			
7a	2.50	496	−6.45	−3.30	3.15	393
7e[14b]	2.65	468	−7.12	−3.76	3.36	369
7g	2.67	464	−7.23	−3.83	3.40	365

[a]Computed using time-dependent DFT (linear response, non-equilibrium solvation).

The absorption and emission properties of BF_2 formazanate complexes **7a,e,g** varied significantly, and involve both the HOMO and LUMO orbitals. While both the HOMO/LUMO for **7a** were significantly higher in energy than those found for complexes **7e,g**, destabilization of the HOMO, due to the extended π conjugation associated with the 3-phenyl substituent, is the dominating factor that leads to red-shifting of its absorption and emission spectra relative to **7e,g**. Although one cannot expect quantitative agreement between HOMO−LUMO gaps and lowest electronic excitation energies, we note that the observed trends in λ_{max} and λ_{em} are consistent with the trends in calculated HOMO−LUMO gaps in toluene: **7a** (393 nm) > **7e** (369 nm) ≈ **7g** (365 nm).

CONCLUSION

In conclusion, we have described the synthesis and characterization of eight BF_2 formazanate complexes, allowing us to systematically assess the effect of extended π conjugation on the spectroscopic and electrochemical properties of BF_2 formazanate complexes. In general, extending the π conjugation of

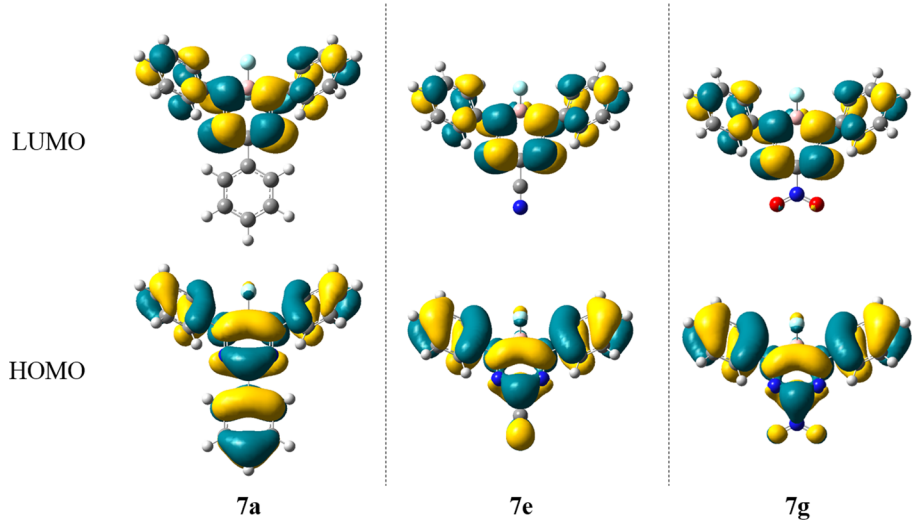

Figure 6. HOMOs and LUMOs for BF_2 complexes **7a** ($Ar_1 = Ar_5 = R_3$ = Ph), **7e** ($Ar_1 = Ar_5$ = Ph, R_3 = CN), and **7g** ($Ar_1 = Ar_5$ = Ph, $R_3 = NO_2$) calculated in toluene solution.

DOI: 10.1021/acs.joc.5b00620
J. Org. Chem. 2015, 80, 5226−5235

complexes by replacing phenyl substituents with naphthyl substituents increased fluorescence quantum yields, increased (less negative) reduction potentials, and red-shifted the wavelengths of maximum absorption and emission. We have also demonstrated the differences in properties between BF_2 complexes of 3-aryl-, 3-cyano-, and 3-nitroformazans relate primarily to the electron-withdrawing nature of the 3-substituents (NO_2 > CN ≫ Ph). The complexes of 3-cyano- and 3-nitroformazans have significantly increased emission quantum yields, and their properties are very sensitive to extension of their π systems. Our future work in this area will focus on the incorporation of BF_2 formazanate complexes into functional polymers with further extended π conjugation.

EXPERIMENTAL SECTION

General Considerations. All reactions and manipulations were carried out under a nitrogen atmosphere using standard Schlenk techniques unless otherwise stated. Solvents were obtained from commercial sources, purified using a standard solvent purification system, collected under vacuum, and stored under a nitrogen atmosphere over 4 Å molecular sieves. The synthesis and characterization of formazans **8a**[16c] and **8e,g**[16d] and BF_2 complex **7e**[14b] have been reported previously. All other reagents were purchased from commercial sources and used as received.

NMR spectra were recorded on a 400 MHz (^{1}H, 399.8 MHz; ^{11}B, 128.3 MHz; ^{19}F, 376.1 MHz) or 600 MHz (^{1}H, 599.5 MHz; ^{13}C, 150.8 MHz) spectrometer. ^{1}H NMR spectra were referenced to residual $CHCl_3$ (7.26 ppm) or DMSO-d_5 (2.50 ppm), and ^{13}C NMR spectra were referenced to $CDCl_3$ (77.2 ppm), CD_2Cl_2 (53.8 ppm), or DMSO-d_6 (39.5 ppm). ^{11}B spectra were referenced to $BF_3{\cdot}OEt_2$ at 0 ppm, and ^{19}F spectra were referenced to $CFCl_3$ at 0 ppm. Mass spectrometry data were recorded in positive-ion mode using electron impact ionization and electrospray ionization. UV−vis absorption data were obtained by running four separate concentrations for each sample, and molar extinction coefficients were determined from the slope of a plot of absorbance against concentration. Infrared spectra were recorded on a KBr disk. Fluorescence spectra were collected for degassed solutions using a commercial spectrophotometer. Excitation wavelengths for the emission spectra were chosen on the basis of λ_{max} values from the respective UV−vis absorption spectrum in the same solvent. Quantum yields were estimated relative to ruthenium tris(bipyridine) hexafluorophosphate by previously described methods and corrected for wavelength-dependent detector sensitivity (Figure S29 in the Supporting Information).[19,20]

Electrochemical Methods. Cyclic voltammograms were recorded using a commercial potentiostat. Electrochemical cells consisted of a three-electrode setup including a glassy-carbon working electrode, platinum-wire counter electrode, and silver-wire pseudo reference electrode. Experiments were run at scan rates of 100 mV s^{-1} in degassed acetonitrile solutions of the analyte (∼1 mM) and supporting electrolyte (0.1 M tetrabutylammonium hexafluorophosphate). Cyclic voltammograms were referenced against an internal standard (∼1 mM ferrocene) and corrected for internal cell resistance using commercial software.

X-ray Crystallography Details. Single crystals of complex **7g** suitable for X-ray diffraction studies were grown by slow evaporation of a concentrated dichloromethane solution. The sample was mounted on a Mitegen polyimide micromount with a small amount of Paratone N oil. All X-ray measurements were made at a temperature of 110 K. The data collection strategy included a number of ω and φ scans which collected data over a range of 2θ angles. The frame integration was performed using SAINT.[24] The resulting raw data were scaled and absorption was corrected using a multiscan averaging of symmetry-equivalent data using SADABS.[25] The structures were solved by direct methods using the XS program.[26] All non-hydrogen atoms were obtained from the initial solution. The hydrogen atoms were introduced at idealized positions and were allowed to refine isotropically. The structural model was fit to the data using full-matrix least squares based on F^2. The calculated structure factors included corrections for anomalous dispersion from the usual tabulation. The structure was refined using the SHELXL-2014 program from SHELXTL.[27] See Table 5 for additional crystallographic data.

Representative Procedure for the Preparation of Formazans 8b,c. *Formazan **8b** (Ar_1 = Ar_5 = Ph, R_3 = Np).* In air, phenylhydrazine (0.69 g, 0.63 mL, 6.4 mmol) was dissolved in ethanol (15 mL). 2-Naphthylaldehyde (1.00 g, 6.40 mmol) was then added, and the solution was stirred for 10 min. After this time, a light yellow precipitate had formed. Dichloromethane (50 mL) and water (50 mL) were added to form a biphasic reaction mixture. Sodium carbonate (2.17 g, 20.5 mmol) and tetrabutylammonium bromide (0.21 g, 0.64 mmol) were added, and the mixture was cooled in an ice bath to 0 °C. In a separate flask, aniline (0.60 g, 6.4 mmol) and concentrated hydrochloric acid (1.6 mL) were mixed in water (15 mL) and cooled in an ice bath. A cooled solution of sodium nitrite (0.51 g, 7.4 mmol) in water (5 mL) was added slowly to the amine solution. This mixture was stirred at 0 °C for 30 min, after which time it was added dropwise to the biphasic reaction mixture described above over 10 min. The resulting solution was stirred for 18 h, which gradually turned dark red over this time. The dark red organic fraction was then washed with deionized water (3 × 50 mL), dried over $MgSO_4$, gravity filtered, and concentrated in vacuo. The resulting residue was purified by flash chromatography (dichloromethane, neutral alumina) to afford formazan **8b** as a dark red microcrystalline solid. Yield: 1.11 g, 50%. Melting point: 124−126 °C. ^{1}H NMR (599.5 MHz, $CDCl_3$): δ 15.49 (s, 1H), 8.62 (s, 1H), 8.29−8.28 (m, 1H), 7.95−7.87 (m, 3H), 7.74 (d, $^3J_{HH}$ = 8 Hz, 4H), 7.52−7.48 (m, 6H), 7.33−7.30 (m, 2H). ^{13}C{^{1}H} NMR (100.6 MHz, $CDCl_3$): δ 148.0, 141.1, 135.0, 133.7, 133.1, 129.5, 128.6, 128.0, 127.7, 127.6, 126.1, 125.9, 124.7, 124.1, 118.9. FT-IR (KBr): 3267 (br, s), 3055 (s), 026 (m), 2915 (m), 2846 (m), 1598 (s), 1501 (s), 1453 (m), 1348 (m), 1253 (s), 1226 (s) cm^{-1}. UV−vis (toluene): λ_{max} 498 nm (ε = 10100 M^{-1} cm^{-1}). MS (EI, +ve mode): exact mass calculated for $[C_{23}H_{18}N_4]^+$, 350.1532; exact mass found, 350.1537; difference, +1.6 ppm.

*Formazan **8c** (Ar_1 = R_3 = Ph, Ar_5 = Np).* In air, from 6.98 mmol of hydrazine/aldehyde: Yield: 2.24 g, 92%. Melting point: 140−142 °C. ^{1}H NMR (400.1 MHz, $CDCl_3$): δ 15.56 (s, 1H), 8.21 (d, $^3J_{HH}$ = 7 Hz, 2H), 8.04 (s, 1H), 7.93−7.88 (m, 3H), 7.85−7.83 (m, 1H), 7.69 (d, $^3J_{HH}$ = 8 Hz, 2H), 7.56−7.47 (m, 6H), 7.43−7.40 (m, 1H), 7.31−7.28

Table 5. X-ray Diffraction Data Collection and Refinement Details for BF_2 Complex 7g

chemical formula	$C_{13}H_{10}BF_2N_5O_2{\cdot}C_{0.50}HCl$
formula wt	359.53
crystal habit	red prism
crystal system	monoclinic
space group	$P2_1/n$
T (K)	110
λ (Å)	0.71073
a (Å)	9.555(8)
b (Å)	17.226(11)
c (Å)	18.840(14)
α (deg)	90
β (deg)	98.070(13)
γ (deg)	90
V (Å^3)	3070(4)
Z	8
ρ (g/cm^3)	1.556
μ (cm^{-1})	0.290
R1,[a] wR2[b] ($I > 2\sigma$)	0.0588, 0.1730
R1, wR2 (all data)	0.0811, 0.1901
GOF[c]	1.025

[a]$R1 = \sum(|F_o| - |F_c|)/\sum F_o$. [b]$wR2 = [\sum(w(F_o^2 - F_c^2)^2)/\sum(wF_o^4)]^{1/2}$. [c]$GOF = [\sum(w(F_o^2 - F_c^2)^2)/((\text{no. of rflns}) - (\text{no. of params}))]^{1/2}$.

DOI: 10.1021/acs.joc.5b00620
J. Org. Chem. 2015, 80, 5226−5235

(m, 1H). $^{13}C\{^1H\}$ NMR (100.6 MHz, $CDCl_3$): δ 147.4, 146.4, 141.4, 137.6, 134.0, 133.3, 129.6, 129.5, 128.5, 128.5, 128.1, 127.8, 127.1, 127.0, 126.5, 126.0, 120.1, 118.5, 116.5. FT-IR (KBr): 3242 (br, s), 3050 (m), 3021 (m), 2915 (m), 2847 (m), 1597 (m), 1515 (m), 1494 (s), 1445 (m), 1348 (m), 1227 (s) cm^{-1}. UV−vis (toluene): λ_{max} 508 nm (ε = 16500 M^{-1} cm^{-1}). MS (EI, +ve mode): exact mass calculated for $[C_{23}H_{18}N_4]^+$, 350.1532; exact mass found, 350.1537; difference, +1.6 ppm.

Preparation of Formazan 8d (Ar_1 = Ar_5 = Np, R_3 = Ph). In air, phenylpyruvic acid (0.51 g, 3.1 mmol) was dissolved in 150 mL of deionized water with sodium hydroxide (0.94 g, 23 mmol) and cooled in an ice bath for 30 min. In a separate flask, 2-naphthylamine (1.00 g, 6.98 mmol) and concentrated hydrochloric acid (1.7 mL) were mixed in water (15 mL) and cooled in an ice bath for 10 min. A cooled solution of sodium nitrite (0.55 g, 8.0 mmol) in water (5 mL) was added slowly to the amine solution. This mixture was stirred at 0 °C for 30 min, after which time it was added dropwise to the phenylpyruvic acid reaction mixture described above over a 10 min period. The resulting solution was stirred for 18 h, during which time a dark purple precipitate was formed. The dark purple solid was filtered off and purified by flash chromatography (dichloromethane, neutral alumina) to afford formazan **8d** as a dark purple microcrystalline solid. Yield: 1.03 g, 82%. Melting point: 152−154 °C. ^1H NMR (599.5 MHz, $CDCl_3$): δ 15.72 (s, 1H), 8.24 (d, $^3J_{HH}$ = 7 Hz, 2H), 8.12 (s, 2H), 7.97−7.91 (m, 6H), 7.87 (d, $^3J_{HH}$ = 8 Hz, 2H), 7.56−7.47 (m, 6H), 7.42−7.38 (m, 1H). $^{13}C\{^1H\}$ NMR (100.6 MHz, $CDCl_3$): δ 145.8, 141.8, 137.6, 134.1, 133.1, 129.7, 128.6, 128.4, 128.2, 127.9, 127.1, 126.3, 126.2, 119.1, 116.5. FT-IR (KBr): 3267 (br, s), 3050 (s), 3034 (m), 2914 (m), 2847 (m), 1629 (m), 1596 (s), 1499 (s), 1438 (m), 1358 (m), 1226 (s) cm^{-1}. UV−vis (toluene): λ_{max} 532 nm (ε = 10300 M^{-1} cm^{-1}). MS (EI, +ve mode): exact mass calculated for $[C_{27}H_{20}N_4]^+$, 400.1688; exact mass found, 400.1695; difference, +1.8 ppm.

Preparation of Formazan 8f (Ar_1 = Ar_5 = Np, R_3 = CN). In air, cyanoacetic acid (0.30 g, 3.5 mmol) was dissolved in 150 mL of deionized water with sodium hydroxide (1.40 g, 34.9 mmol) and cooled in an ice bath. In a separate flask, 2-naphthylamine (1.00 g, 6.98 mmol) and concentrated hydrochloric acid (1.7 mL) were mixed in water (15 mL) and cooled in an ice bath. A cooled solution of sodium nitrite (0.55 g, 8.0 mmol) in water (5 mL) was added slowly to the amine solution. This mixture was stirred at 0 °C for 30 min, after which time it was added dropwise to the cyanoacetic acid solution described above over a 10 min period. The resulting solution was stirred for 18 h, during which time a dark red precipitate was formed. The dark red solid was filtered off and purified by flash chromatography (dichloromethane, neutral alumina) to afford formazan **8f** as a dark red microcrystalline solid. Yield: 1.06 g, 86%. Melting point: 187−189 °C. ^1H NMR (599.5 MHz, DMSO-d_6): δ 12.90 (s, 1H), 8.39 (s, 2H), 8.18−7.88 (m, 8H), 7.62−7.51 (m, 4H). $^{13}C\{^1H\}$ NMR (100.6 MHz, DMSO-d_6): δ 144.9, 133.3, 132.7, 129.5, 128.6, 127.9, 127.8, 127.2, 127.0, 126.7, 116.5, 112.9. FT-IR (KBr): 3276 (br, m), 3053 (m), 2970 (m), 2219 (s), 1604 (s), 1531 (s), 1367 (m), 1346 (m), 1267 (m) cm^{-1}. UV−vis (toluene): λ_{max} 472 nm (ε = 12, 900 M^{-1} cm^{-1}). MS (EI, +ve mode): exact mass calculated for $[C_{22}H_{15}N_5]^+$, 349.1327; exact mass found, 349.1330; difference, +0.7 ppm.

Preparation of Formazan 8h (Ar_1 = Ar_5 = Np, R_3 = NO_2). In air, nitromethane (0.21 g, 0.19 mL, 3.5 mmol) was dissolved in 100 mL of deionized water with sodium hydroxide (0.31 g, 7.7 mmol) and cooled in an ice bath. In a separate flask, 2-naphthylamine (1.00 g, 6.98 mmol) and concentrated hydrochloric acid (1.7 mL) were mixed in water (15 mL) and cooled in an ice bath. A cooled solution of sodium nitrite (0.55 g, 8.0 mmol) in water (5 mL) was added slowly to the amine solution. This mixture was stirred at 0 °C for 30 min, after which time it was added dropwise to the nitromethane solution described above over a 10 min period. The resulting solution was stirred for 18 h, during which time a dark red precipitate was formed. The dark red solid was filtered off and purified by flash chromatography (dichloromethane, neutral alumina) to afford formazan **8h** as a dark red microcrystalline solid. Yield: 0.35 g, 27%. Melting point: 179−181 °C. ^1H NMR (599.5 MHz, $CDCl_3$): δ 15.63 (s, 1H), 8.18 (s, 2H), 8.00−7.96 (m, 6H), 7.90 (d, $^3J_{HH}$ = 7 Hz, 2H), 7.60−7.56 (m, 4H). $^{13}C\{^1H\}$ NMR (100.6 MHz, CD_2Cl_2): δ 144.5, 134.3, 133.9, 130.6, 129.1, 128.5, 127.9, 125.8, 122.0, 116.3, 110.4. FT-IR (KBr): 3242 (br, s), 3035 (m), 2915 (m), 2857 (m), 1589 (m), 1547 (s), 1502 (m), 1342 (s), 1277 (s) cm^{-1}. UV−vis (toluene): λ_{max} 488 nm (ε = 12, 500 M^{-1} cm^{-1}). MS (EI, +ve mode): exact mass calculated for $[C_{21}H_{15}N_5O_2]^+$, 369.1226; exact mass found, 369.1220; difference, −1.6 ppm. This compound decomposes over several hours in halogenated solvents.

Representative Procedure for the Preparation of Formazanate BF_2 Complexes 7a−h. *Formazanate BF_2 Complex **7a** (Ar_1 = R_3 = Ar_5 = Ph).* Formazan **8a** (0.50 g, 1.6 mmol) was dissolved in dry toluene (50 mL). Triethylamine (0.50 g, 0.68 mL, 4.9 mmol) was then added slowly, and the solution was stirred for 10 min. Boron trifluoride diethyl etherate (1.16 g, 1.01 mL, 8.15 mmol) was then added, and the solution was heated at 80 °C for 18 h. The solution gradually turned from dark red to dark purple during this time. The reaction mixture was then cooled to 20 °C and deionized water (10 mL) was added to quench any excess reactive boron-containing compounds. The red-purple toluene solution was then washed with deionized water (3 × 50 mL), dried over $MgSO_4$, gravity-filtered, and concentrated in vacuo. The resulting residue was purified by flash chromatography (dichloromethane, neutral alumina) to afford BF_2 complex **7a** as a dark purple microcrystalline solid. Yield: 0.38 g, 67%. Melting point: 129−131 °C. ^1H NMR (599.5 MHz, $CDCl_3$): δ 8.12 (d, $^3J_{HH}$ = 7 Hz, 2H), 7.92 (d, $^3J_{HH}$ = 7 Hz, 4H), 7.50−7.43 (m, 9H). $^{13}C\{^1H\}$ NMR (100.6 MHz, $CDCl_3$): δ 143.9, 133.6, 129.7, 129.3, 129.1, 128.8, 125.5, 123.5 (t, $^4J_{CF}$ = 3 Hz). ^{11}B NMR (128.3 MHz, $CDCl_3$): δ −0.6 (t, $^1J_{BF}$ = 29 Hz). ^{19}F NMR (376.1 Hz, $CDCl_3$): δ −144.6 (q, $^1J_{FB}$ = 29 Hz). FT-IR (KBr): 3263 (m), 3035 (m), 2900 (m), 2889 (m), 1310 (m), 1290 (s), 1265 (s), 1218 (m), 1168 (m), 1113 (s) cm^{-1}. UV−vis (toluene): λ_{max} 517 nm (ε = 23800 M^{-1} cm^{-1}). MS (EI, +ve mode): exact mass calculated for $[C_{19}H_{15}N_4BF_2]^+$, 348.1358; exact mass found, 348.1374; difference, +4.7 ppm.

*Formazanate BF_2 Complex **7b** (Ar_1 = Ar_5 = Ph, R_3 = Np).* From 1.70 mmol of formazan **8b**. Yield: 0.31 g, 46%. Melting point: 127−129 °C. ^1H NMR (599.5 MHz, $CDCl_3$): δ 8.56 (s, 1H), 8.27−8.25 (m, 1H), 7.96−7.93 (m, 6H), 7.90−7.88 (m, 1H), 7.54−7.50 (m, 6H), 7.48−7.45 (m, 2H). $^{13}C\{^1H\}$ NMR (100.6 MHz, $CDCl_3$): δ 144.0, 134.0, 133.6, 131.1, 129.9, 129.3, 128.8, 128.7, 128.0, 126.8, 126.7, 125.1, 123.7 (t, $^4J_{CF}$ = 4 Hz), 123.1, 110.2. ^{11}B NMR (128.3 MHz, $CDCl_3$): δ −0.5 (t, $^1J_{BF}$ = 29 Hz). ^{19}F NMR (376.1 Hz, $CDCl_3$): δ −144.8 (q, $^1J_{FB}$ = 29 Hz). FT-IR (KBr): 3236 (m), 3055 (m), 2915 (m), 2860 (m), 1313 (s), 1279 (s), 1220 (m), 1172 (m), 1106 (m), 1105 (m) cm^{-1}. UV−vis (toluene): λ_{max} 529 nm (ε = 20900 M^{-1} cm^{-1}). MS (EI, +ve mode): exact mass calculated for $[C_{23}H_{17}N_4BF_2]^+$, 398.1514; exact mass found, 398.1513; difference, −0.3 ppm.

*Formazanate BF_2 Complex **7c** (Ar_1 = R_3 = Ph, Ar_5 = Np).* From 1.50 mmol of formazan **8c**: Yield: 0.44 g, 73%. Melting point: 106−108 °C. ^1H NMR (599.5 MHz, $CDCl_3$): δ 8.46 (s, 1H), 8.18−8.16 (m, 2H), 8.07−8.05 (m, 1H), 7.97−7.92 (m, 4H), 7.88−7.86 (m, 1H), 7.57−7.43 (m, 8H). $^{13}C\{^1H\}$ NMR (100.6 MHz, $CDCl_3$): δ 149.4, 144.1, 141.6, 133.8, 133.6, 133.2, 129.8, 129.5, 129.3, 129.3, 129.2, 128.9, 127.9, 127.8, 127.2, 125.7, 123.6 (t, $^4J_{CF}$ = 2 Hz), 123.4 (t, $^4J_{CF}$ = 4 Hz), 120.7. ^{11}B NMR (128.3 MHz, $CDCl_3$): δ −0.4 (t, $^1J_{BF}$ = 29 Hz). ^{19}F NMR (376.1 Hz, $CDCl_3$): δ −143.9 (q, $^1J_{FB}$ = 29 Hz). FT-IR (KBr): 3236 (m), 3059 (s), 2915 (m), 2845 (m), 1347 (m), 1341 (m), 1294 (s), 1266 (s), 1218 (m), 1174 (m) cm^{-1}. UV−vis (toluene): λ_{max} 535 nm (ε = 26800 M^{-1} cm^{-1}). MS (EI, +ve mode): exact mass calculated for $[C_{23}H_{17}N_4BF_2]^+$, 398.1514; exact mass found, 398.1512; difference, −0.6 ppm.

*Formazanate BF_2 Complex **7d** (Ar_1 = Ar_5 = Np, R_3 = Ph).* From 2.70 mmol of formazan **8d**: Yield: 0.95 g, 78%. Melting point: 140−142 °C. ^1H NMR (599.5 MHz, $CDCl_3$): δ 8.49 (s, 2H), 8.21 (d, $^3J_{HH}$ = 7 Hz, 2H), 8.10−8.08 (m, 2H), 7.97−7.93 (m, 4H), 7.89−7.86 (m, 2H), 7.57−7.48 (m, 7H). $^{13}C\{^1H\}$ NMR (100.6 MHz, $CDCl_3$): δ 141.6, 133.9, 133.5, 133.1, 129.4, 129.3, 129.3, 128.9, 127.9, 127.7, 127.1, 125.7, 123.3 (t, $^4J_{CF}$ = 4 Hz), 120.6, 119.1. ^{11}B NMR (128.3 MHz, $CDCl_3$): δ −0.2 (t, $^1J_{BF}$ = 29 Hz). ^{19}F NMR (376.1 Hz, $CDCl_3$):

DOI: 10.1021/acs.joc.5b00620
J. Org. Chem. 2015, 80, 5226−5235

δ −143.3 (q, $^1J_{FB}$ = 29 Hz). FT-IR (KBr): 3276 (m), 3050 (s), 2915 (m), 2846 (m), 1626 (m), 1592 (m), 1507 (s), 1344 (s), 1298 (s), 1265 (m) cm^{-1}. UV−vis (toluene): λ_{max} 556 nm (ε = 25200 M^{-1} cm^{-1}). MS (ESI, +ve mode): exact mass calculated for $[C_{27}H_{19}N_4BF_2Na]^+$, 471.1568; exact mass found, 471.1569; difference, +0.1 ppm.

Formazanate BF_2 Complex ***7f*** *(Ar_1 = Ar_5 = Np, R_3 = CN).* From 2.30 mmol of formazan **8f**: Yield: 0.74 g, 81%. Melting point: 118−120 °C. ^{1}H NMR (599.5 MHz, $CDCl_3$): δ 8.51 (s, 2H), 8.03−8.01 (m, 2H), 7.98−7.93 (m, 4H), 7.89−7.87 (m, 2H), 7.62−7.56 (m, 4H). ^{13}C{^{1}H} NMR (100.6 MHz, $CDCl_3$): δ 141.0, 134.4, 133.1, 130.1, 129.9, 129.0, 128.2, 127.8, 126.4, 124.2, 119.5 (t, $^4J_{CF}$ = 3 Hz), 114.5. ^{11}B NMR (128.3 MHz, $CDCl_3$): δ −0.4 (t, $^1J_{BF}$ = 31 Hz). ^{19}F NMR (376.1 Hz, $CDCl_3$): δ −132.7 (q, $^1J_{FB}$ = 31 Hz). FT-IR (KBr): 3235 (m), 3035 (m), 2895 (m), 2240 (s), 1350 (s), 1146 (m), 1124 (m), 1028 (m) cm^{-1}. UV−vis (toluene): λ_{max} 581 nm (ε = 25700 M^{-1} cm^{-1}). MS (EI, +ve mode): exact mass calculated for $[C_{22}H_{14}N_5BF_2]^+$, 397.1310; exact mass found, 397.1311; difference, +0.2 ppm.

Formazanate BF_2 Complex ***7g*** *(Ar_1 = Ar_5 = Ph, R_3 = NO_2).* From 2.90 mmol of formazan **8g**: Yield: 0.27 g, 29%. Melting point: 108−110 °C. ^{1}H NMR (399.8 MHz, $CDCl_3$): δ 8.01−7.99 (m, 4H), 7.56−7.52 (m, 6H). ^{13}C{^{1}H} NMR (100.6 MHz, $CDCl_3$): δ 143.4, 132.2, 129.9, 123.7 (t, $^4J_{CF}$ = 2 Hz). ^{11}B NMR (128.3 MHz, $CDCl_3$): δ −0.7 (t, $^1J_{BF}$ = 30 Hz). ^{19}F NMR (376.1 Hz, $CDCl_3$): δ −135.4 (q, $^1J_{FB}$ = 29 Hz). FT-IR (KBr): 3257 (m), 3062 (m), 2915 (m), 2912 (m), 2844 (m), 1557 (s), 1417 (s), 1333 (s), 1327 (s), 1271 (m), 1175 (m), 1151 (m) cm^{-1}. UV−vis (toluene): λ_{max} 505 nm (ε = 26000 M^{-1} cm^{-1}). MS (EI, +ve mode): exact mass calculated for $[C_{13}H_{10}N_5O_2BF_2]^+$, 317.0896; exact mass found, 317.0901; difference, +1.7 ppm.

Formazanate BF_2 Complex ***7h*** *(Ar_1 = Ar_5 = Np, R_3 = NO_2).* From 0.54 mmol of formazan **8h**: Yield: 0.22 g, 99%. Melting point: 199−201 °C. ^{1}H NMR (599.5 MHz, $CDCl_3$): δ 8.61 (s, 2H), 8.14 (d, $^3J_{HH}$ = 9 Hz, 2H), 8.01−7.97 (m, 4H), 7.90 (d, $^3J_{HH}$ = 8 Hz, 2H), 7.65−7.58 (m, 4H). ^{13}C{^{1}H} NMR (100.6 MHz, $CDCl_3$): δ 141.1, 134.6, 133.1, 130.4, 130.3, 129.9, 129.2, 128.2, 127.8, 124.6 (t, $^4J_{CF}$ = 4 Hz), 119.5. ^{11}B NMR (128.3 MHz, $CDCl_3$): δ −0.3 (t, $^1J_{BF}$ = 29 Hz). ^{19}F NMR (376.1 Hz, $CDCl_3$): δ −134.3 (q, $^1J_{FB}$ = 29 Hz). FT-IR (KBr): 3270 (s), 3036 (m), 2888 (m), 1554 (s), 1538 (m), 1425 (m), 1377 (m), 1317 (s), 1269 (w) cm^{-1}. UV−vis (toluene): λ_{max} 583 nm (ε = 24100 M^{-1} cm^{-1}). MS (EI, +ve mode): exact mass calculated for $[C_{21}H_{14}N_5O_2BF_2]^+$, 417.1209; exact mass found, 417.1208; difference, −0.24 ppm.

■ ASSOCIATED CONTENT

Supporting Information

Figures, tables, and CIF files giving ^{1}H and ^{13}C NMR spectra, UV−vis absorption and emission spectra, cyclic voltammograms, computational details and crystallographic data for **7g**. The Supporting Information is available free of charge on the ACS Publications website at DOI: 10.1021/acs.joc.5b00620.

■ AUTHOR INFORMATION

Corresponding Author

*J.B.G.: e-mail, joe.gilroy@uwo.ca; tel, +1-519-661-2111 ext. 81561.

Notes

The authors declare no competing financial interest.

■ ACKNOWLEDGMENTS

This work was supported by the Natural Sciences and Engineering Research Council (NSERC) of Canada Discovery Grants (J.B.G. and V.N.S.) and Canada Graduate Scholarships program (S.M.B.) and by The University of Western Ontario. We thank Prof. Elizabeth R. Gillies for access to instruments in her lab.

■ REFERENCES

(1) Murov, S. L. *Handbook of Photochemistry*; Marcel Dekker: New York, 1973.

(2) Roncali, J.; Leriche, P.; Blanchard, P. *Adv. Mater.* **2014**, *26*, 3821−3838.

(3) Frath, D.; Massue, J.; Ulrich, G.; Ziessel, R. *Angew. Chem., Int. Ed.* **2014**, *53*, 2290−2310.

(4) Wu, W.; Liu, Y.; Zhu, D. *Chem. Soc. Rev.* **2010**, *39*, 1489−1502.

(5) Mei, J.; Hong, Y.; Lam, J. W. Y.; Qin, A.; Tang, Y.; Tang, B. Z. *Adv. Mater.* **2014**, *26*, 5429−5479.

(6) For example: (a) Qian, B.; Baek, S. W.; Smith, M. R., III *Polyhedron* **1999**, *18*, 2405−2414. (b) Norman, D. W.; Edwards, J. P.; Vogels, C. M.; Decken, A.; Westcott, S. A. *Can. J. Chem.* **2002**, *80*, 31−40. (c) Liddle, B. J.; Silva, R. M.; Morin, T. J.; Macedo, F. P.; Shukla, R.; Lindeman, S. V.; Gardinier, J. R. *J. Org. Chem.* **2007**, *72*, 5637−5646. (d) Kubota, Y.; Tsuzuki, T.; Funabiki, K.; Ebihara, M.; Matsui, M. *Org. Lett.* **2010**, *12*, 4010−4013. (e) Oakley, S. R.; Nawn, G.; Waldie, K. M.; MacInnis, T. D.; Patrick, B. O.; Hicks, R. G. *Chem. Commun.* **2010**, *46*, 6753−6755. (f) Cheng, F.; Jäkle, F. *Chem. Commun.* **2010**, *46*, 3717−3719. (g) Liu, T.; Chien, A. D.; Lu, J.; Zhang, G.; Fraser, C. L. *J. Mater. Chem.* **2011**, *21*, 8401−8408. (h) Bonnier, C.; Machin, D. D.; Abdi, O.; Koivisto, B. D. *Org. Biomol. Chem.* **2013**, *11*, 3756−3760. (i) Kubota, Y.; Ozaki, Y.; Funabiki, K.; Matsui, M. *J. Org. Chem.* **2013**, *78*, 7058−7067. (j) Albrett, A. M.; Thomas, K. E.; Maslek, S.; Młodzianowska, A.; Conradie, J.; Beavers, C. M.; Ghosh, A.; Brothers, P. J. *Inorg. Chem.* **2014**, *53*, 5486−5493. (k) Barbon, S. M.; Staroverov, V. N.; Boyle, P. D.; Gilroy, J. B. *Dalton Trans.* **2014**, *43*, 240−250. (l) Liao, C.-W.; Rajeswara, R. M.; Sun, S.-S. *Chem. Commun.* **2015**, *51*, 2656−2659. (m) Kubota, Y.; Kasatani, K.; Takai, H.; Funabiki, K.; Matsui, M. *Dalton Trans.* **2015**, *44*, 3326−3341.

(7) Reviews: (a) Loudet, A.; Burgess, K. *Chem. Rev.* **2007**, *107*, 4891−4932. (b) Ulrich, G.; Ziessel, R.; Harriman, A. *Angew. Chem., Int. Ed.* **2008**, *47*, 1184−1201. (c) Boens, N.; Leen, V.; Dehaen, W. *Chem. Soc. Rev.* **2012**, *41*, 1130−1172.

(8) For example: (a) Chen, J.; Burghart, A.; Derecskei-Kovacs, A.; Burgess, K. *J. Org. Chem.* **2000**, *65*, 2900−2906. (b) Ueno, Y.; Jose, J.; Loudet, A.; Pérez-Bolívar, C.; Anzenbacher, P.; Burgess, K. *J. Am. Chem. Soc.* **2011**, *133*, 51−55. (c) Niu, S.; Ulrich, G.; Retailleau, P.; Ziessel, R. *Tetrahedron Lett.* **2011**, *52*, 4848−4853. (d) Nepomnyashchii, A. B.; Bröring, M.; Ahrens, J.; Bard, A. J. *J. Am. Chem. Soc.* **2011**, *133*, 8633−8645. (e) Lu, J.-s.; Ko, S.-B.; Walters, N. R.; Wang, S. *Org. Lett.* **2012**, *14*, 5660−5663. (f) Zhang, X.; Yu, H.; Xiao, Y. *J. Org. Chem.* **2012**, *77*, 669−673. (g) Jameson, L. P.; Dzyuba, S. V. *Bioorg. Med. Chem. Lett.* **2013**, *23*, 1732−1735. (h) Manjare, S. T.; Kim, J.; Lee, Y.; Churchill, D. G. *Org. Lett.* **2014**, *16*, 520−523. (i) Frenette, M.; Hatamimoslehabadi, M.; Bellinger-Buckley, S.; Laoui, S.; La, J.; Bag, S.; Mallidi, S.; Hasan, T.; Bouma, B.; Yelleswarapu, C.; Rochford, J. *J. Am. Chem. Soc.* **2014**, *136*, 15853−15856. (j) Shie, J.-J.; Liu, Y.-C.; Lee, Y.-M.; Lim, C.; Fang, J.-M.; Wong, C.-H. *J. Am. Chem. Soc.* **2014**, *136*, 9953−9961. (k) Bandi, V.; Das, S. K.; Awuah, S. G.; You, Y.; D'Souza, F. *J. Am. Chem. Soc.* **2014**, *136*, 7571−7574. (l) Bruhn, T.; Pescitelli, G.; Jurinovich, S.; Schaumlöffel, A.; Witterauf, F.; Ahrens, J.; Bröring, M.; Bringmann, G. *Angew. Chem., Int. Ed.* **2014**, *53*, 14592−14595. (m) Raut, S.; Kimball, J.; Fudala, R.; Doan, H.; Maliwal, B.; Sabnis, N.; Lacko, A.; Gryczynski, I.; Dzyuba, S. V.; Gryczynski, Z. *Phys. Chem. Chem. Phys.* **2014**, *16*, 27037−27042. (n) Lakshmi, V.; Ravikanth, M. *RSC Adv.* **2014**, *4*, 44327−44336.

(9) Kollmannsberger, M.; Rurack, K.; Resch-Genger, U.; Daub, J. *J. Phys. Chem. A* **1998**, *102*, 10211−10220.

(10) Shen, Z.; Röhr, H.; Rurack, K.; Uno, H.; Spieles, M.; Schulz, B.; Reck, G.; Ono, N. *Chem. - Eur. J.* **2004**, *10*, 4853−4871.

(11) Quan, L.; Chen, Y.; Lv, X.-J.; Fu, W.-F. *Chem. - Eur. J.* **2012**, *18*, 14599−14604.

(12) Araneda, J. F.; Piers, W. E.; Heyne, B.; Parvez, M.; McDonald, R. *Angew. Chem., Int. Ed.* **2011**, *50*, 12214−12217.

(13) Reviews: (a) Nineham, A. W. *Chem. Rev.* **1955**, *55*, 355−483. (b) Sigeiken, G. I.; Lipunova, G. N.; Pervova, I. G. *Russ. Chem. Rev.* **2006**, *75*, 885−900.

DOI: 10.1021/acs.joc.5b00620
J. Org. Chem. 2015, 80, 5226−5235

(14) (a) Chang, M.-C.; Otten, E. *Chem. Commun.* **2014**, *50*, 7431−7433. (b) Barbon, S. M.; Reinkeluers, P. A.; Price, J. T.; Staroverov, V. N.; Gilroy, J. B. *Chem. - Eur. J.* **2014**, *20*, 11340−11344. (c) Barbon, S. M.; Price, J. T.; Reinkeluers, P. A.; Gilroy, J. B. *Inorg. Chem.* **2014**, *53*, 10585−10593.
(15) Hesari, M.; Barbon, S. M.; Staroverov, V. N.; Ding, Z.; Gilroy, J. B. *Chem. Commun.* **2015**, *51*, 3766−3769.
(16) (a) Ibrahim, Y. A.; Elwahy, A. H. M.; Abbas, A. A. *Tetrahedron* **1994**, *50*, 11489−11498. (b) Katritzky, A. A.; Belyakov, S. A.; Cheng, D.; Durst, H. D. *Synthesis* **1995**, *1995*, 577−581. (c) Gilroy, J. B.; McKinnon, S. D. J.; Koivisto, B. D.; Hicks, R. G. *Org. Lett.* **2007**, *9*, 4837−4840. (d) Gilroy, J. B.; Otieno, P. O.; Ferguson, M. J.; McDonald, R.; Hicks, R. G. *Inorg. Chem.* **2008**, *47*, 1279−1286.
(17) Gilroy, J. B.; Ferguson, M. J.; McDonald, R.; Patrick, B. O.; Hicks, R. G. *Chem. Commun.* **2007**, 126−128.
(18) For example: (a) Gilroy, J. B.; Ferguson, M. J.; McDonald, R.; Hicks, R. G. *Inorg. Chim. Acta* **2008**, *361*, 3388−3393. (b) Gilroy, J. B.; Patrick, B. O.; McDonald, R.; Hicks, R. G. *Inorg. Chem.* **2008**, *47*, 1287−1294. (c) Hong, S.; Gupta, A. K.; Tolman, W. B. *Inorg. Chem.* **2009**, *48*, 6323−6325. (d) Hong, S.; Hill, L. M. R.; Gupta, A. K.; Naab, B. D.; Gilroy, J. B.; Hicks, R. G.; Cramer, C. J.; Tolman, W. B. *Inorg. Chem.* **2009**, *48*, 4514−4523. (e) Lipunova, G. N.; Rezinskikh, Z. G.; Maslakova, T. I.; Slepukhin, P. A.; Pervova, I. G.; Lipunov, I. N.; Sigeikin, G. I. *Russ. J. Coord. Chem.* **2009**, *35*, 215−221. (f) Zaidman, A. V.; Pervova, I. G.; Vilms, A. I.; Belov, G. P.; Kayumov, R. R.; Slepukhin, P. A.; Lipunov, I. N. *Inorg. Chim. Acta* **2011**, *367*, 29−34. (g) Chang, M.-C.; Dann, T.; Day, D. P.; Lutz, M.; Wildgoose, G. G.; Otten, E. *Angew. Chem. Int. Ed.* **2014**, *53*, 4118−4122. (h) Travieso-Puente, R.; Chang, M.-C.; Otten, E. *Dalton Trans.* **2014**, *43*, 18035−18041. (i) Chang, M.-C.; Roewen, P.; Travieso-Puente, R.; Lutz, M.; Otten, E. *Inorg. Chem.* **2015**, *54*, 379−388.
(19) Fery-Forgues, S.; Lavabre, D. *J. Chem. Educ.* **1999**, *76*, 1260−1264.
(20) Suzuki, K.; Kobayashi, A.; Kaneko, S.; Takehira, K.; Yoshihara, T.; Ishida, H.; Shiina, Y.; Oishi, S.; Tobita, S. *Phys. Chem. Chem. Phys.* **2009**, *11*, 9850−9860.
(21) *CRC Handbook of Chemistry and Physics*; CRC Press: Boca Raton, FL, 2012.
(22) Frisch, M. J.; Trucks, G. W.; Schlegel, H. B.; Scuseria, G. E.; Robb, M. A.; Cheeseman, J. R.; Scalmani, G.; Barone, V.; Mennucci, B.; Petersson, G. A.; Nakatsuji, H.; Caricato, M.; Li, X.; Hratchian, H. P.; Izmaylov, A. F.; Bloino, J.; Zheng, G.; Sonnenberg, J. L.; Hada, M.; Ehara, M.; Toyota, K.; Fukuda, R.; Hasegawa, J.; Ishida, M.; Nakajima, T.; Honda, Y.; Kitao, O.; Nakai, H.; Vreven, T.; Montgomery, J. A., Jr.; Peralta, J. E.; Ogliaro, F.; Bearpark, M.; Heyd, J. J.; Brothers, E.; Kudin, K. N.; Staroverov, V. N.; Kobayashi, R.; Normand, J.; Raghavachari, K.; Rendell, A.; Burant, J. C.; Iyengar, S. S.; Tomasi, J.; Cossi, M.; Rega, N.; Millam, J. M.; Klene, M.; Knox, J. E.; Cross, J. B.; Bakken, V.; Adamo, C.; Jaramillo, J.; Gomperts, R.; Stratmann, R. E.; Yazyev, O.; Austin, A. J.; Cammi, R.; Pomelli, C.; Ochterski, J. W.; Martin, R. L.; Morokuma, K.; Zakrzewski, V. G.; Voth, G. A.; Salvador, P.; Dannenberg, J. J.; Dapprich, S.; Daniels, A. D.; Farkas, Ö.; Foresman, J. B.; Ortiz, J. V.; Cioslowski, J.; Fox, D. J. *Gaussian 09, Revision B.01*; Gaussian, Inc., Wallingford, CT, 2009.
(23) Zhao, Y.; Truhlar, D. G. *Theor. Chem. Acc.* **2008**, *120*, 215−241.
(24) *SAINT version 2013.8*; Bruker-AXS, Madison, WI 53711, USA, 2013.
(25) *SADABS version 2012.1*; Bruker-AXS, Madison, WI 53711, USA, 2012.
(26) Sheldrick, G. M. *Acta Crystallogr.* **2015**, *A71*, 3−8.
(27) Sheldrick, G. M. *Acta Crystallogr.* **2008**, *A64*, 112−122.

DOI: 10.1021/acs.joc.5b00620
J. Org. Chem. 2015, 80, 5226−5235